Light propagation in a cylindrical waveguide with a complex, metallic, dielectric function

L. Novotny* and C. Hafner
Swiss Federal Institute of Technology, CH-8092 Zürich, Switzerland
(Received 5 July 1994)

Motivated by problems in scanning near-field optical microscopy, we discuss light propagation in circular dielectric waveguides with finite aluminum cladding. In order to understand the origin of the different solutions, optical modes are first investigated for the dielectric waveguide with infinite aluminum cladding and for the aluminum cylinder. For aluminum a plasma dispersion law is assumed, leading to complex dielectric constants with negative real parts and to generally complex propagation constants. The dependence of the dispersion on the geometry and on the frequency is discussed for the various kinds of modes. We find that the existence of most of the modes is limited to certain frequencies and geometries, i.e., the solutions have a cutoff in the complex propagation constant plane. Contrary to dielectric waveguide theory, where cutoff describes the abrupt transition from propagating to evanescent modes, no other solution is generated when cutoff of a mode is reached. Surface modes and other kinds of modes, such as guided or bulk modes, can either couple between each other or transform into each other.

PACS number(s): 42.25.Bs, 03.50.De, 41.20.Bt, 41.20.Jb

I. INTRODUCTION

Metal coated optical fibers find an important application in scanning near-field optical microscopy (SNOM) [1,2]. This technique uses a metal coated tapered fiber with an aperture at the end as light emitting probe. It is well known that only a small amount of the input light power reaches the end aperture of the probe. The investigation of this unfavorable effect and the design of optimized SNOM probes require the understanding of light propagation in metal coated optical waveguides.

In this paper we investigate the propagation of guided optical waves in circular waveguides made of concentric layers of glass, aluminum, and vacuum. Although this structure is relatively simple, the classification of the modes and the understanding of the observed effects is far from being trivial. Therefore we reduce the complexity in a first step and discuss (1) guided optical waves of the aluminum cylinder in vacuum and (2) solutions of the dielectric waveguide with infinite aluminum cladding. These two simplified cases are obtained from our initial structure (1) by setting the radius of the glass core equal to zero and (2) by assuming an infinite thickness for the aluminum cladding. The modes found for the simplified structures are used for the classification and discussion of the modes of the initial structure. Two main aspects are emphasized: (1) dependence of the propagation constant on geometrical parameters and (2) frequency dispersion.

For glass, we assume a real, frequency-independent, dielectric constant; whereas for aluminum, we allow for a complex dielectric constant that obeys a plasma dispersion law. At optical wavelengths, the real part of the dielectric constant of aluminum is negative and has therefore a surface active character which leads at certain frequencies to plasmon excitations (resonant density oscillations of the electron gas [3,4]). These resonances depend on the material, frequency, and geometry. Surface modes, such as surface plasmon modes, are localized at the interfaces between different media. In surface and thin film physics, surface plasmons find an important application as sensitive surface probes (optical sensors) for the investigation of surfaces [5].

Several authors discussed solutions of the wave equation for the infinite cylinder with negative dielectric constant. Their attention was mainly focused on cylindrical surface polaritons [6–10]. One of the first experiments to excite optical modes on an aluminum cylinder was performed by Miziumski [11] using light scattering. Pfeiffer, Economou, and Ngai [8] explained these results by means of virtual radiative modes which have a complex frequency and thus a finite lifetime. Virtual radiative modes with frequencies greater than the plasma frequency were investigated by Martinos and Economou [12]. For the case of a lossy metal cylinder irradiated by a plane wave at normal incidence (vanishing propagation constant) they show that the eigenfrequencies correspond to peaks in the absorption spectrum. Recently a systematic classification of all possible guided modes in cylindrical geometry with two concentric media, one of them having a negative dielectric constant, was given by Prade and Vinet [13]. Lossy waveguide structures have been described mainly by means of transmission line theory [14] leading to approximate solutions based on perturbation theory.

In this work, attenuation is associated with the imaginary part of the dielectric constant of aluminum. The propagation constants of the waveguide modes will therefore be complex. A distinction of pure propagating and

*Present address: Swiss Federal Institute of Technology ETH, Laboratory for Field Theory and Microwave Electronics, ETH-Zentrum, CH-8092 Zürich, Switzerland. Fax: +41 1 632 11 98; Electronic address: novotny@ifh.ee.ethz.ch.

pure evanescent modes is no longer possible. Instead there is a transition from more or less propagating to more or less evanescent modes. The coupling between electromagnetic and other forms of energy makes the physical interpretation much more difficult since the analysis must be done with complex parameters. Graphical representation becomes extensive since real and imaginary parts have to be shown simultaneously.

The paper is organized as follows. Section II outlines waveguide theory and the methods used for this work. For a waveguide with dielectric core and infinite aluminum cladding we investigate in Sec. III the dependence of the propagation constant on the core radius and frequency. A similar study is done in Sec. IV for an aluminum cylinder surrounded by vacuum. Finally we discuss in Sec. V the modes of a waveguide with dielectric core and finite aluminum cladding by using the results of the preceding sections.

II. THEORY

Throughout this paper we assume a real frequency, determined by the time-harmonic excitation. Pseudonormal modes, obtained by other authors for complex frequencies [8], are therefore not investigated here. The solution of Maxwell's equations in cylindrical structures is well documented in the literature [15]. Therefore we emphasize only some aspects of the derivation of the waveguide modes. The field $\mathbf{F}\in\{\mathbf{E},\mathbf{H}\}$ pròpagates along the waveguide axis z as

$$\mathbf{F}(\rho,\varphi,z)=\mathbf{F}(\rho,\phi)e^{i(k_z z-\omega t)}, \tag{1}$$

where k_z is the propagation constant and ρ,φ are polar coordinates in the transverse plane. For the complex propagation constant we use the following notation:

$$k_z=\beta+i\alpha\ . \tag{2}$$

In Eq. (2) β is the phase constant and α the attenuation constant. Real and imaginary parts of dielectric constants will be denoted as

$$\varepsilon=\varepsilon'+i\varepsilon''\ , \tag{3}$$

where $\sqrt{\varepsilon}$ is the index of refraction. In the (ρ,φ) plane, we consider two or three concentric domains from which only one has a complex dielectric constant. The azimuthal dependence of the fields in each domain is described by harmonic functions $\sin(n\varphi)$, $\cos(n\varphi)$ of order n and the radial dependence by cylinder functions that fulfill a second order Bessel differential equation. In the inner domain only a Bessel function of the first kind, J_n, can be used in order to have a finite solution along the waveguide axis. For the outermost domain, on the other hand, only a Hankel function of the first kind, $H_n^{(1)}$, may be applied in order to fulfill the radiation condition at infinity. A closed domain which does not contain the waveguide axis is described by two linearly independent cylinder functions.

The argument of a cylinder function in domain D_i reads $(\kappa_i\rho)$ where κ_i is the transverse wave number. κ_i is related to κ_z by

$$\kappa_i^2=k_0^2\left[\varepsilon_i-\left[\frac{k_z}{k_0}\right]^2\right], \tag{4}$$

where k_0 is the free space wave number: $k_0=\omega/c$. When taking the square root of (4) we obtain two values for κ_i. It is important to note that for $H_n^{(1)}$ in the outermost domain, the value of κ_i with positive imaginary part must always be taken in order to satisfy the radiation condition.

On each boundary separating two domains D_i,D_j at $\rho=R_{ij}$, four continuity conditions for the tangential components of the electric and magnetic fields can be formulated. Imposing that the determinant of the resulting homogeneous system of equations must vanish, we obtain the transcendental equation

$$\det[M(k_z)]=0 \tag{5}$$

for the complex propagation constant k_z. M is the resulting matrix of the system of equations. For a physical system with L layers, the size of this matrix is $4(L-1)$. For order $n=0$ the matrix can be split into two independent submatrices of size $2(L-1)$ corresponding to TE and TM solutions. For complex dielectric constants the value of the determinant is complex too and Eq. (5) must be fulfilled for real and imaginary parts simultaneously. In that case, $|\det[M(k_z)]|=0$, which can be used as a criterion for the determination of k_z.

We have used two independent procedures for the determination of the propagation constant. In the first one we wrote a code to determine the minima of $|\det[M(k_z)]|$ as a function of k_z. This code is based on routines of the NAG FORTRAN library [16]. A minimum with a value at least 20 orders of magnitude smaller than the average value of $|\det[M(k_z)]|$ was identified as a mode. The second procedure relied on the two dimensional (2D) multiple multipole program (MMP) for waves on arbitrary cylindrical structures [17]. In this method an overdetermined system of equations is used. The error in the boundary conditions is evaluated as a function of k_z and a mode is associated with the minimum of this error. The results of both methods agreed up to the eighth digit.

A. Classification of modes and idealization of models

A general purpose computer code such as 2D MMP can easily find a large number of modes propagating in a cylindrical structure. For the code there are no essential differences between the modes. Therefore a simple enumeration seems to be appropriate; but a classification containing some interesting information is helpful for understanding the mechanisms of wave propagation in cylindrical structures. Such a classification is usually based on a complete analytic solution that is known for sufficiently simple geometries only. Here it is important to note that "analytic" solutions usually lead to transcendental equations that cannot be solved analytically. In order to distinguish this kind of solution from pure numerical solutions based on a discretization, we keep the term "analytical."

The classification of modes on geometrically complicated structures that cannot be determined analytically is tricky and somehow ambiguous. Since one often is interested in the coupling of a complex structure with a simpler one, one tries to establish classification on the complex structure based on the known classification of the simpler structure. The same is done even in our case of a cladded circular fiber, where analytic solutions are known. Therefore we start with the examination of the two special cases (1) zero diameter of the dielectric core and (2) infinite cladding. Afterwards, we use the classification of the special cases to describe the modes of a structure with finite core and finite cladding.

For a dielectric waveguide with a loss-free metal cladding (hollow metal waveguide) one distinguishes TE*nm* and TM*nm* modes. The index n of the circular structure denotes the angular symmetry of the mode and the index m denotes the radial dependence of the field. For the modes of the corresponding rectangular waveguide one has the same notation with a different meaning of the indices n and m. On an ideal step-index fiber most of the modes are hybrid and only the $n=0$ modes are transverse. Since hybrid modes are often almost TM or almost TE modes, one distinguishes EH*nm* and HE*nm* modes. This distinction can be misleading because the dominance of some field components strongly depends on the material properties, on the geometry, and on the frequency.

Loss-free models are often used for the classification of modes for reasons of simplicity. To obtain such a model, one can either neglect the conductivity of a material or one can assume an infinite conductivity. The solutions and classifications obtained in both cases are completely different. When a complex model with finite conductivity is studied, one usually uses the same classification as in the ideal case that is closer to the actual situation. For frequency-dependent materials this can cause transitions from one mode into another one. Such a transition is somehow fictitious as it is the name of the mode rather than the mode itself which changes. We will study such transitions in Sec. V.

Ignoring losses has another consequence: most of the modes have a finite cutoff frequency. Their propagation constant is real above the cutoff frequency, which indicates that the waves propagate without any attenuation. The propagation constant becomes imaginary below the cutoff frequency and the modes are called evanescent. In the following sections we will observe a transition from "propagating" modes to "evanescent" modes in an area where the loss-free model shows cutoff. Surprisingly, we find another "true" cutoff for most of the modes. This cutoff is usually considerably below the cutoff of the idealized model. Below the idealized model cutoff there is still a solution (the evanescent wave) of the problem posed, but below the "true" cutoff there is no solution at all. It can be shown that the "true" cutoff frequency tends toward zero if the losses tend toward zero.

In models with frequency-independent materials, the scaling of the geometric data is equivalent to the scaling of the frequency. The plots of the propagation constant versus the radius of a fiber and the plots of the propagation constants versus the frequency are almost identical. Consequently, one obtains a cutoff radius corresponding to the cutoff frequency. An explicit computation of the dependence on the radius is not required. The mode in our investigation is neither loss-free nor frequency independent. Therefore, we will separately consider the dependence of the propagation constants on the radius and on the frequency.

B. Frequency dispersion

For wavelengths shorter than $\lambda \approx 800$ nm, the dielectric function of aluminum is very well described by the plasma dispersion law [18]

$$\varepsilon_{\text{alu}}(\omega)=1-\frac{\omega_p^2}{\omega^2+i\gamma\omega}\ , \tag{6}$$

where the plasma frequency is given by $\hbar\omega_p=15.565$ eV and the damping constant by $\hbar\gamma=0.608$ eV. At $\lambda\approx 800$ nm experimental aluminum data deviate from the dispersion law (6) because of interband excitations of inner core electrons. With an additional Lorentzian resonance superposed to (6) it is easy to account for this bound electron effect. Although we could directly use an interpolation of measured data in our numerical analysis, we will use (6) for reasons of simplicity. For glass we assume a real, frequency-independent dielectric constant $\varepsilon_{\text{glass}}=2.16$. Although in this paper we sometimes consider structures smaller than 10 nm, we do not take spatial dispersion into account, i.e., the electron gas has no compressibility. It is therefore assumed that energy is transported completely by electromagnetic waves and by no other mechanism. A nonlocal discussion of cylindrical surface modes based on a hydrodynamic model can be found in Ref. [7].

III. MODES OF A DIELECTRIC WAVEGUIDE WITH INFINITE METAL CLADDING

A. Dependence on core radius

In this section we consider a dielectric core with variable radius R surrounded by an infinite aluminum cladding. Although a strict distinction between propagating and evanescent modes cannot be achieved, we will nevertheless use these expressions. Figure 1 shows β and α for the first 12 modes as a function of R at a fixed wavelength of $\lambda=488$ nm. At this wavelength the dielectric constant of aluminum is $\varepsilon_{\text{alu}}=-34.5+i8.5$. Note that a logarithmic scale is used in Fig. 1(b). As R decreases the modes run continuously from a propagating through a transition to an evanescent region. In the propagating region the attenuation of some modes decays faster than those of others. At $R=300$ nm, for example, the TE01 mode shows the lowest attenuation. The modes in the propagating region are similar to those of the hollow metal waveguide for which completely transverse modes are obtained. The sequence of modes of the hollow metal waveguide starts with TE11, TM01, TE21; whereas for the aluminum coated waveguide we obtain the sequence HE11, TM01, HE21. The next two modes of the hollow

metal waveguide, TM11 and TE01, are degenerate. The corresponding modes of the aluminum waveguide, EH11 and TE01, are not degenerate but similar. Especially in the transition region they have almost identical values of k_z (Fig. 1). For all modes the attenuation changes rapidly from $\approx 0.07k_0$ to $\approx 0.7k_0$ in the transition region and becomes more or less an exponential function of R in the evanescent region.

1. Small core radius

An interesting result is that all the modes, with the exception of the HE11 modes vanish when R becomes smaller than a critical value, i.e., they have a cutoff (Fig. 1). Note that cutoff in dielectric waveguide theory describes the abrupt transition from pure propagating to pure evanescent modes. When damping is included, this transition becomes continuous and the term cutoff becomes vague. In the following we therefore distinguish between cutoff and transition of a mode. The disappearance of a mode shall be denoted as cutoff.

The situation near cutoff can be better analyzed when looking at Fig. 2, which shows a parametric plot in the complex k_z plane with R taken as parameter. All TM and EH modes, i.e., modes with a large magnetic field in the transverse plane, have a cutoff when $\beta=0$. Mathematically, these solutions would continue with negative values of β but since such solutions do not fulfill energy conservation, they are excluded from the discussion. At cutoff, the propagation constants of all the investigated TM and EH modes are close to $k_z \approx i4k_0$ (the deviation is less than 2.5%). This cutoff value depends only slightly on $\varepsilon_{\text{glass}}$ but is rather sensitive to ε_{alu}. For each TM and EH mode, we calculated the cutoff radius (R_c), i.e., the radius for which $k_z = k_{z\,(\text{cutoff})}$ crosses the imaginary axis. We then calculated k_z for a lossless structure ($\text{Im}\{\varepsilon_{\text{alu}}\}=0$) with the same radius R_c. Rather surprisingly, the obtained k_z value was always within 0.025% identical with $k_{z\,(\text{cutoff})}$. In other words, at cutoff, TM and EH modes are almost identical to the corresponding modes of the lossless waveguide. Note, however, that for increasing values of $\text{Im}\{\varepsilon_{\text{alu}}\}$ the deviation between the two k_z also increases.

TE and HE modes, i.e., modes with a large electric field in the transverse plane, have on principle a different behavior. In the evanescent region, before reaching cutoff, their phase constants increase for decreasing R. Cutoff is reached when k_z reaches the curve described by

$$2\alpha\beta = \varepsilon''_{\text{alu}} k_0^2 \quad \text{and} \quad \beta^2 - \alpha^2 < \varepsilon'_{\text{alu}} k_0^2 \, . \tag{7}$$

This is the curve where $\text{Im}\{\kappa_{\text{alu}}\}=0$ and the arguments of the Hankel functions describing the radial dependence of the fields in aluminum become real. This means that near

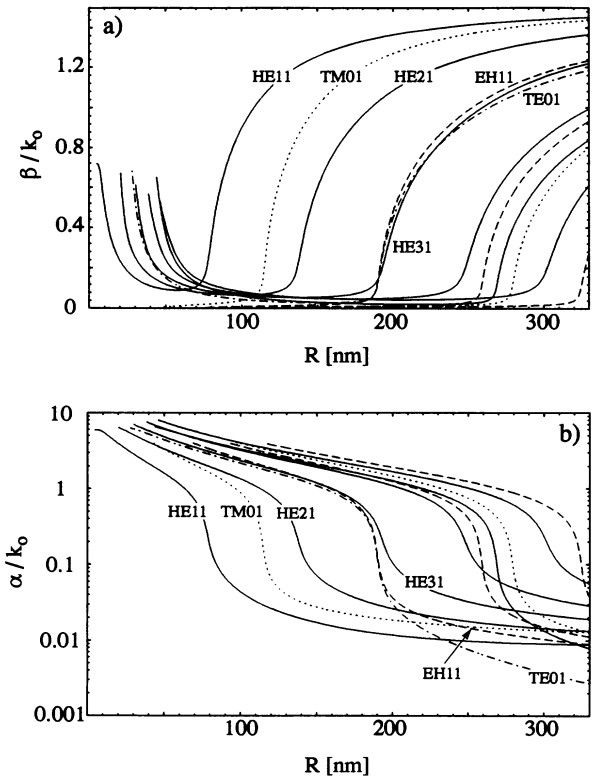

FIG. 1. Propagation constant as a function of core radius R. For decreasing R the modes run from a propagating through a transitional to an evanescent region. The modes disappear when they reach cutoff. Wavelength $\lambda=488$ nm; infinite aluminum cladding $\varepsilon=-34+i8.5$; dielectric core $\varepsilon=2.16$. HE modes, solid lines; EH modes, dashed lines; TE modes, dash-dotted lines; TM modes, dotted lines.

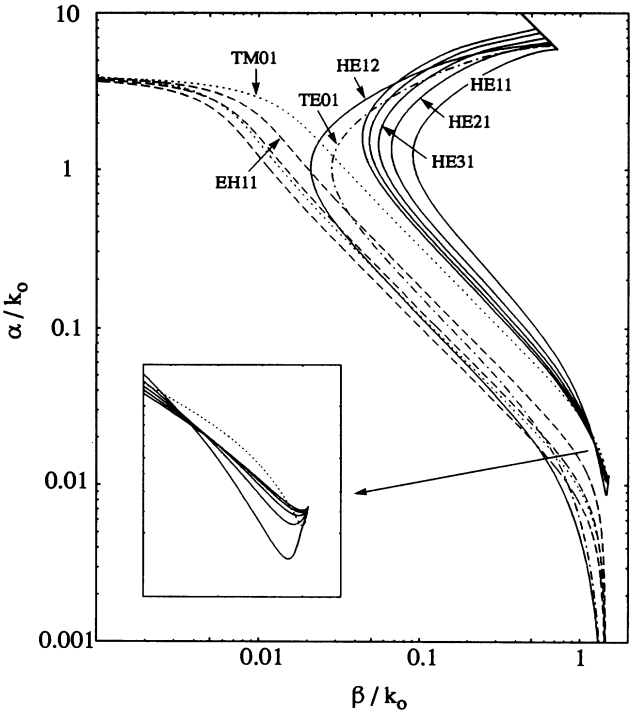

FIG. 2. Parametric plot of the propagation constants (the core radius is the parameter). The thick solid line indicates $\text{Im}\{\kappa_{\text{alu}}\}=0$. Wavelength $\lambda=488$ nm; infinite aluminum cladding $\varepsilon=-34+i8.50$; dielectric core $\varepsilon=2.16$; HE modes, solid lines; EH modes, dashed lines; TE modes, dash-dotted lines; TM modes, dotted lines.

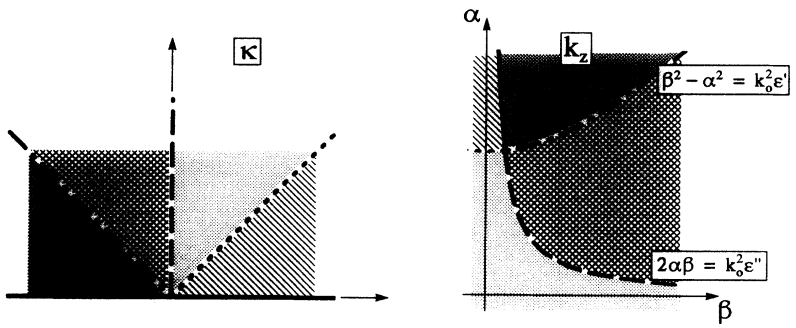

FIG. 3. Transformation from transverse wave number κ to propagation constant $k_z=\alpha+i\beta$.

cutoff the fields in the aluminum cladding have oscillatory behavior in the transverse plane and decay with ρ^{-n}. Hankel functions are discontinuous for negative real arguments [19]. Since the negative and the positive real κ axis are transformed on the same curve (7) in the k_z plane (Fig. 3) the modes reach cutoff when the Hankel functions become discontinuous. The transformation from the complex κ to the complex k_z plane is sketched in Fig. 3. In Fig. 4 the absolute value of the determinant (5) is evaluated in the complex k_z plane for $R=20.5$ nm. The minimum in the figure corresponds to the HE21 mode when reaching cutoff.

The HE11 mode asymptotically approaches $k_z=k_0\sqrt{\varepsilon_{\text{alu}}}$, which is equivalent to $\kappa_{\text{alu}}=0$. We suppose that the HE11 mode has no cutoff. This is not easy to verify numerically since for $R\to 0$ also κ_{alu} tends to zero and the argument of the Hankel function becomes very small. However, it is interesting to note that below a certain R no other mode or no other homogeneous solution to Maxwell's equations than the HE11 mode exist. In a metal coated tapered waveguide one solution after the other will therefore vanish as the radius decreases. At the end only the HE11 solution will still exist. This is not the case in the theory of loss-free dielectric waveguides

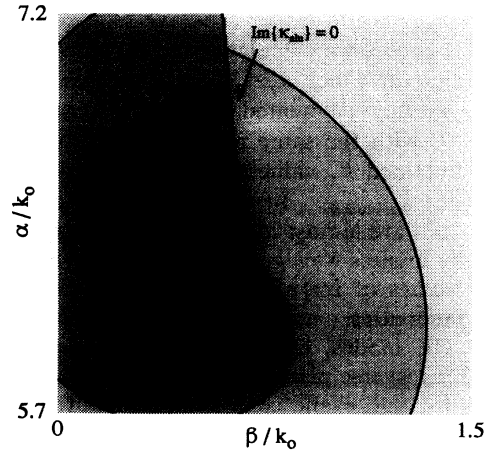

FIG. 4. Lines of constant $|\det[M(k_z)]|$. Core radius $R=20.5$ nm; wavelength $\lambda=488$ nm; infinite aluminum cladding $\varepsilon=-34+i8.5$; dielectric core $\varepsilon=2.16$. The minimum corresponds to the HE21 mode when reaching cutoff. The discontinuity indicates $\text{Im}\{\kappa_{\text{alu}}\}=0$.

where always an infinite set of evanescent solutions is predicted and cutoff of a pure propagating mode is accompanied by the creation of a pure evanescent mode that has no cutoff.

2. *Large core radius*

In loss-free waveguides it is possible to distinguish between oscillatory modes (guided modes) and surface type modes [13]. The field amplitudes of the latter are maximum at the interface. To obtain such a field distribution in the core, the Bessel functions must monotonically increase towards the interface. This is obtained for imaginary arguments. Real arguments lead to radially oscillating modes. In the lossy case it is no longer possible to distinguish between pure oscillatory and pure surface types of modes because the arguments are always complex. The classification into these two types of modes turns out to be a problem similar to the distinction between evanescent and propagating modes. At a planar interface between a dielectric and a metal described by a complex dielectric constant with negative real part, nonradiative surface modes (lossy Fano modes) are obtained if the condition

$$|\varepsilon_{\text{alu}}|>2\varepsilon_{\text{diel}} \tag{8}$$

is satisfied. At $\lambda=488$ nm the cylindrical configuration fulfills condition (8) so that for certain R the existence of surface modes may be expected. Indeed, for large R, we find two different asymptotic limits for k_z (Fig. 2). As expected from the theory of optical waveguides, most of the modes tend towards the limit

$$k_z=k_0\sqrt{\varepsilon_{\text{glass}}}\,. \tag{9}$$

However, the TM01 mode and HEn1 modes have a limit at

$$k_z=k_0\left[\frac{\varepsilon_{\text{glass}}\varepsilon_{\text{alu}}}{\varepsilon_{\text{glass}}+\varepsilon_{\text{alu}}}\right]^{1/2}, \tag{10}$$

which is the dispersion relation for surface plasmons at planar interfaces [4]. At the plasmon frequency, where $\varepsilon_{\text{alu}}\approx-\varepsilon_{\text{glass}}$, k_z becomes very large; in the absence of damping even infinite. Note that before reaching the limiting value (10), the parametric k_z curves of the HEn1 and TM01 modes intersect in almost the same point. In the limit $R\to\infty$ surface modes have finite attenuation whereas guided modes propagate without losses. The re-

sult that some guided modes become surface modes when R is increasing is rather surprising. Moreover, for a given order n there is only one existing surface mode. This uniqueness was also observed in Ref. [13] in the absence of damping. No TE surface mode can exist since the electric field of TE modes is oriented circularly around the waveguide axis and therefore parallel to the interface. For TM modes, on the other hand, the electric field in the transverse plane points toward the waveguide axis and is perpendicular to the interface. A net surface charge can thus be generated. As we will see in Sec. IV, the same types of surface modes are also found for the aluminum cylinder. Note that the power in the cladding can flow in opposite direction to the power in the core. The direction of the net power flux, however, is always determined by the core.

B. Frequency dispersion

For the following discussion we use the plasma dispersion law (6). At frequencies below $\omega=0.1\omega_p$ the results will not be representative for aluminum since the influence of bound electrons is neglected. According to the discussion above, the modes can be categorized into two different groups: HEn1 and TM01 modes which become surface modes for increasing R and guided modes. In the following we discuss frequency dispersion for a mode of each group. The propagation of light in a homogeneous space consisting of the core material is represented in Figs. 5(a) and 6(a) by the dash-dotted core line.

In Fig. 5 dispersion curves for the HE12 guided mode are shown for five different radii R. Two regions can be distinguished: a propagating and an evanescent one. For high enough frequencies all modes are propagating and asymptotically approach the core line from the left side. Their phase velocity, defined as ω/β, is therefore higher than the phase velocity of light propagating in an infinite core medium. The larger R is, the closer the dispersion curves to the core line are. For low ω, in the evanescent region, the propagation lengths of the modes, defined as $1/\alpha$, become very short. A mode has a cutoff if condition (7) can be fulfilled. Note that the behavior of the HE12 mode is representative for all the other modes that remain guided for large radius R.

Dispersion curves of the HE11 modes are shown in Fig. 6. For comparison, the dispersion curves for a planar interface (10) are shown by dotted lines. Since we allow for damping, these curves deviate considerably from the familiar dispersion curves in the literature. Accounting for damping causes continuous transition from nonradiative surface modes (Fano modes) to radiative surface modes (Brewster modes). As a consequence, the dispersion curve bends back at frequencies near the plasmon frequency. This backbending effect was verified experimentally with measurements using the attenuated total reflection (ATR) technique [20] and discussed by several authors [21,22]. Over its entire spectrum, a HE11 mode passes through different characteristic states. For low ω it behaves like an evanescent mode. As ω increases it becomes a propagating mode. Rather surprisingly, the dispersion curve then crosses the core line and becomes a nonradiative surface mode approaching the plasmon frequency. Then, the dispersion curve bends back and α increases, causing a very short propagation length. For all R the surface modes couple back into evanescent modes, which is characterized by the near-circular α curves. This coupling can be rather abrupt as seen for $R=200$ nm when following the α curve. For some values of R the modes at large ω become propagating modes, for other values they run into cutoff and disappear. Note that the curve for $R=200$ nm is already close to the plasmon dispersion curve of the planar interface. The smaller the radius R is, the higher the resonance frequency is. Other modes which become surface modes for large R behave similarly to the HE11 mode.

IV. OPTICAL MODES OF A METAL CYLINDER

Modes propagating on the surface of a metal wire characterized by a small dielectric constant and finite conductivity were investigated already at the beginning of the century [23]. These Zenneck type modes extend in the surrounding vacuum over large distances, i.e., k_z is close to k_0. At optical wavelengths where metals are

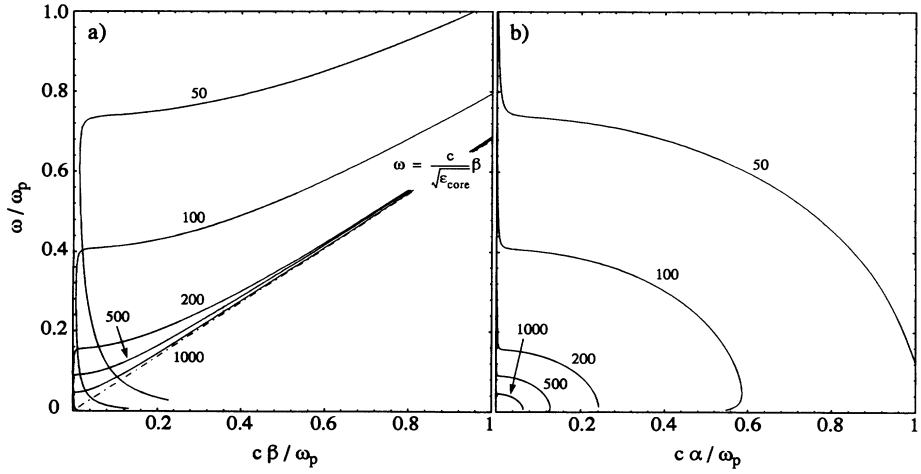

FIG. 5. Frequency dispersion of the HE12 mode for different core radius. The numbers specify the core radius in nm. Infinite aluminum cladding $\hbar\omega_p=15.565$ eV, $\hbar\gamma=0.608$ eV; dielectric core $\varepsilon=2.16$.

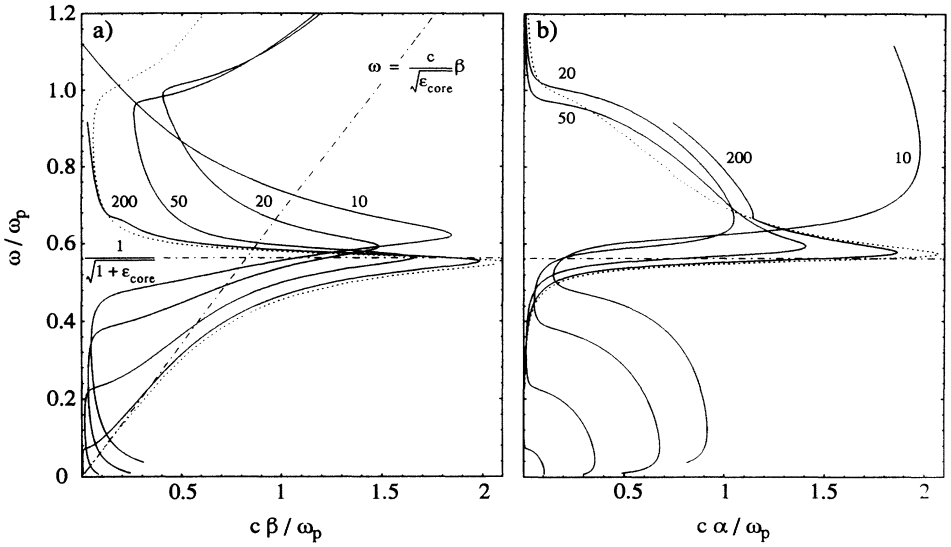

FIG. 6. Frequency dispersion of the HE11 mode for different core radii. The numbers specify the core radii in nm. The surface plasmon dispersion of the corresponding planar interface is indicated by dotted lines. Infinite aluminum cladding $\hbar\omega_p = 15.565$ eV, $\hbar\gamma = 0.608$ eV; dielectric core $\varepsilon = 2.16$.

characterized by negative dielectric constants surface modes can become strongly localized to the boundaries and form a surface plasmon. For lossless cylinders, surface plasmon modes have been discussed in the literature by several authors [6–10,13]. They can be either radiative or nonradiative [24,8].

A. Dependence on radius

1. Small radius

In Fig. 7 the propagation constants of the first two surface modes are shown as a function of the radius of the aluminum wire. For each order n we find only one solution, that is, a TM0 mode for $n=0$ and a HEn mode for $n \geq 1$. In the limit of small R the propagation constant of the TM0 mode tends to infinity, which is in accordance with Ref. [13] where lossless media were considered. However, the smaller R is, the faster the radial field decay in the surrounding vacuum is. In the aluminum core the field radially decays more slowly and the amount of electromagnetic energy propagating inside the wire increases. The attenuation of the TM0 mode therefore increases and the propagation length tends to zero.

Similarly to the discussion of the preceding section, we observe for HEn surface modes cutoffs when

$$\mathrm{Im}\{\kappa_{vac}\} = 0 \ . \tag{11}$$

Condition (11) can be fulfilled if

$$\beta = 0 \tag{12}$$

or if

$$\alpha = 0 \quad \text{and} \quad 0 < \beta < k_0 \ . \tag{13}$$

For decreasing R the HE1 surface mode asymptotically approaches

$$k_z = k_0 \ , \tag{14}$$

which corresponds to an unattenuated wave with a radially infinite extension. For $R \to 0$ higher order surface modes convert to radiating ones, since at cutoff the transverse wave number κ_{vac} becomes real. For the aluminum wire at $\lambda = 488$ nm the cutoff values of the HE2 and the HE3 mode are $k_z = 0.9968 k_0$ at $R = 418$ nm and $k_z = 0.9917 k_0$ at $R = 725$ nm, respectively.

In a second class of modes the fields are distributed over the interior of the wire and therefore have high attenuation. They are similar to the guided modes discussed in the preceding section. In the following we shall call them bulk modes. Their dependence on R is shown in Fig. 8. Except the TM01 mode, all other bulk modes have a cutoff described by (12), i.e., cutoff is reached when the modes become purely evanescent. Similarly to the corresponding surface mode, the TM01 mode approaches an infinite k_z value for small R. For all bulk

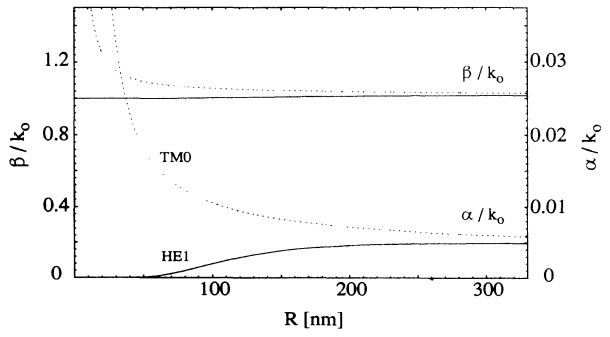

FIG. 7. Propagation constants of the lowest two surface modes as a function of cylinder radius R. Wavelength $\lambda = 488$ nm; aluminum cylinder $\varepsilon = -34 + i8.5$; surrounded by vacuum. Phase and attenuation constants are drawn in the same figure.

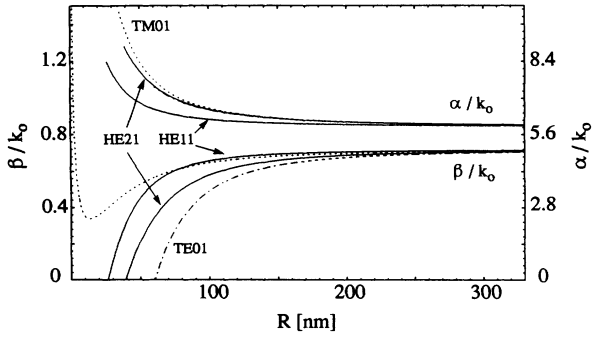

FIG. 8. Propagation constants of the first few bulk modes as a function of cylinder radius R. Wavelength $\lambda=488$ nm; aluminum cylinder $\varepsilon=-34+i8.5$; surrounded by vacuum. Phase and attenuation constants are drawn in the same figure.

modes it is observed that the smaller R is, the higher the attenuation is. The contrary could be expected since the absorbing area is smaller for smaller R.

2. *Large radius*

In Fig. 9 a parametric plot of the first four surface modes is shown. In the asymptotic limit the surface plasmon solution must be recovered. Therefore, for $R\rightarrow\infty$ all the curves end in the same point, given by

$$k_z=k_0\left[\frac{\varepsilon_{\text{alu}}}{1+\varepsilon_{\text{alu}}}\right]^{1/2}. \tag{15}$$

For $R\rightarrow\infty$ bulk modes asymptotically reach the value (Fig. 10)

$$k_z=k_0\sqrt{\varepsilon_{\text{alu}}}\,. \tag{16}$$

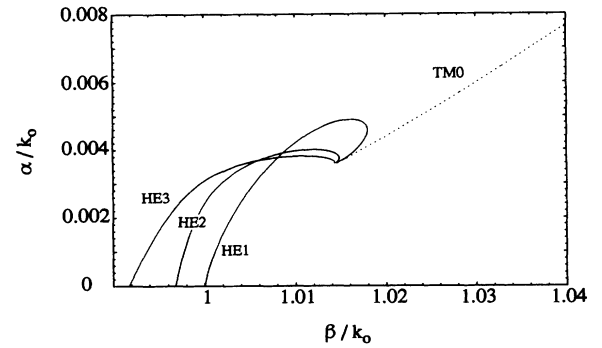

FIG. 9. Parametric plot of the propagation constant for the lowest four surface modes (the cylinder radius is the parameter). Wavelength $\lambda=488$ nm; aluminum cylinder $\varepsilon=-34+i8.5$; surrounded by vacuum.

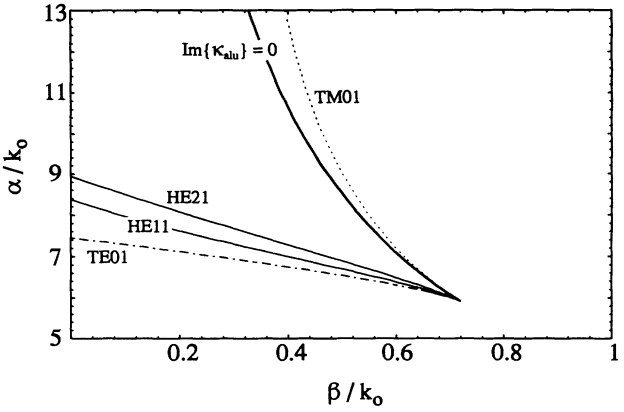

FIG. 10. Parametric plot of the propagation constant for the first few bulk modes (the cylinder radius is the parameter). Wavelength $\lambda=488$ nm; aluminum cylinder $\varepsilon=-34+i8.5$; surrounded by vacuum.

B. Frequency dispersion

Below the plasmon frequency the surface modes of the aluminum cylinder are very similar to those of the planar interface (Fig. 11). For low ω they asymptotically approach the light line which describes propagation of light in free space. For ω close to the plasmon frequency $\omega_p/\sqrt{2}$ the surface modes become strongly localized at the interface. The thinner the cylinder, the larger the propagation constant at the plasmon frequency. Note that these surface modes are much less sensitive to geometrical alterations than those which were obtained for the metal coated dielectric waveguide. Above the plasmon frequency, the surface modes convert very abruptly into bulk modes which have a cutoff when they become purely evanescent, i.e., $\beta\rightarrow 0$. If the cylinder is thick enough, a bulk mode can convert into a propagating mode above the plasma frequency ω_p. This is shown in Fig. 11 for $R=500$ nm. The propagating mode then asymptotically approaches the light line. Bulk modes are characterized by a very short propagation length and two peaks in their β curves (Fig. 12). The shorter the propagation length, the larger the peak near the plasmon frequency and the smaller the peak at low frequencies. Since bulk modes are to the left of the light line (radiative modes) they can simply be excited by light scattering.

Surface modes of different orders are shown in Fig. 13 for a fixed R of 100 nm. Whereas the TM0 and the HE1 mode have no cutoff for low frequencies, higher order modes all have a cutoff determined by the condition (11). Before reaching cutoff, surface modes cross the light line and become radiative. In Fig. 13, cutoff is described by (13) for surface modes with orders lower than $n=7$ and by (12) for surface modes with $n=7$ or higher. For high values of n and small radius R several authors observed a minimum in the dispersion curve [8,13]. Such a minimum, which gives rise to a region with negative group velocity, was not observed in the present investigation. We suppose that the absence of this minimum is due to damping which is taken into account in our analysis.

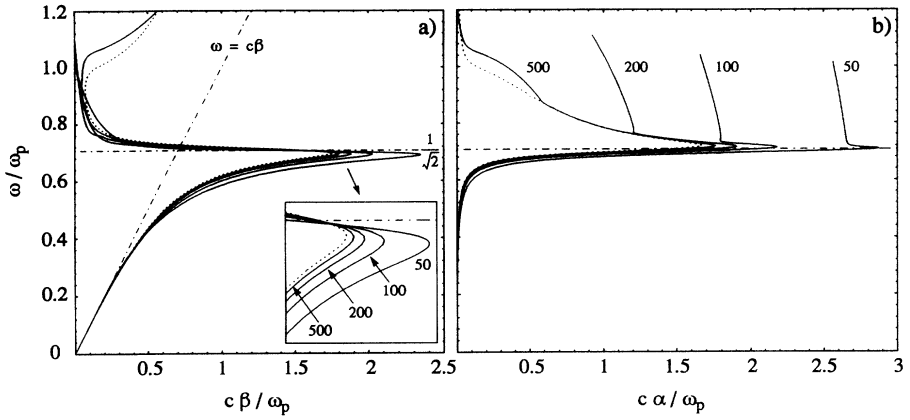

FIG. 11. Frequency dispersion of the HE1 surface mode for different cylinder radii. The numbers specify the cylinder radii in nm. The surface plasmon dispersion of the corresponding planar interface is indicated by dotted lines. Aluminum cylinder $\hbar\omega_p = 15.565$ eV, $\hbar\gamma = 0.608$ eV; surrounded by vacuum.

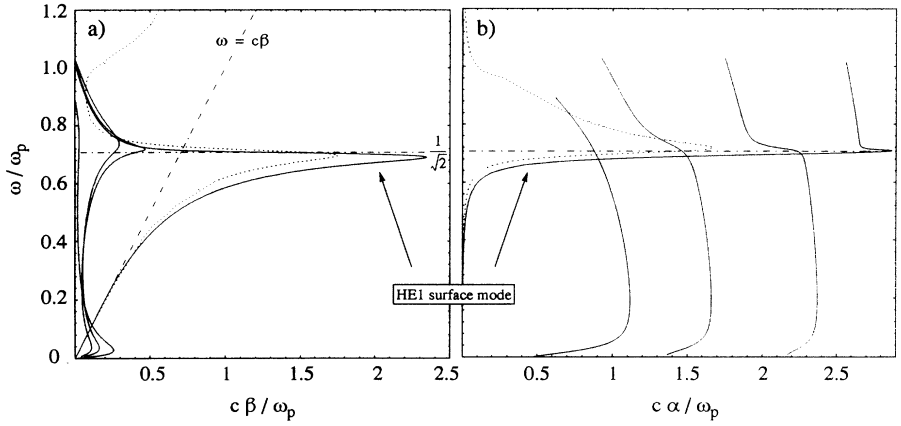

FIG. 12. Frequency dispersion of bulk modes of order $n = 1$ for a cylinder radius $R = 50$ nm. The HE1 surface mode is shown for comparison. The surface plasmon dispersion of the corresponding planar interface is indicated by dotted lines. Aluminum cylinder $\hbar\omega_p = 15.565$ eV, $\hbar\gamma = 0.608$ eV; surrounded by vacuum.

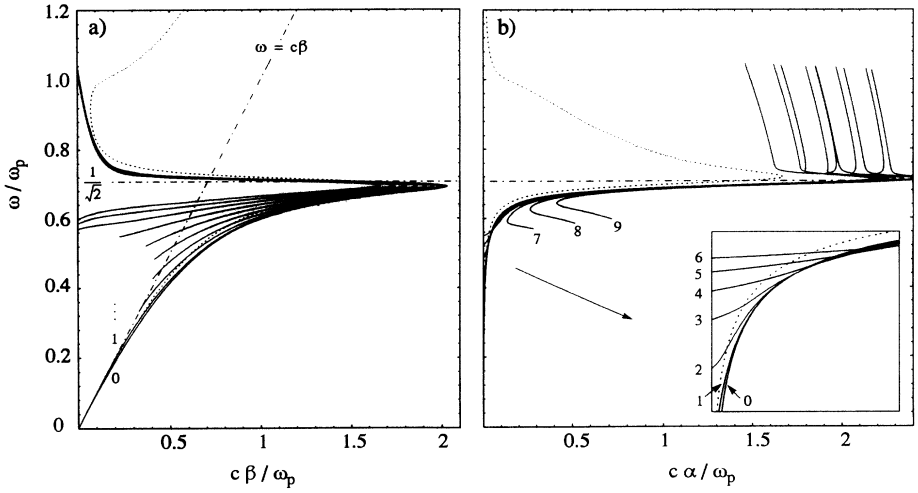

FIG. 13. Frequency dispersion of HEn surface modes for a cylinder radius $R = 100$ nm. The numbers specify the order n. The surface plasmon dispersion of the corresponding planar interface is indicated by dotted lines. Aluminum cylinder $\hbar\omega_p = 15.565$ eV, $\hbar\gamma = 0.608$ eV; surrounded by vacuum.

V. MODES OF A DIELECTRIC WAVEGUIDE WITH METAL CLADDING OF FINITE THICKNESS

The results of the preceding sections were obtained for waveguides consisting of two concentric materials. In this section we shall combine these results by considering a dielectric core with an aluminum cladding of finite thickness D. For this structure three different types of modes may be expected to exist: *guided modes* concentrated to the interior of the dielectric core, *interface modes* localized on the boundary between core and cladding, and *surface modes* tied to the surface of the cladding. As we will see, coupling between the different kinds of modes occurs when their propagation constants come close to each other.

A. Dependence on geometry

For the discussion below we again assume a fixed wavelength of $\lambda=488$ nm. The influence of finite cladding is presented in Fig. 14 where parametric plots for infinite cladding and 50 nm thick cladding are shown. Contrary to Fig. 2 we use here a linear scaling. For large R the curves of the two cases are almost identical. However, for small R a different behavior is observed. This is not surprising since in the limit $R\to 0$ the waveguide consists of an aluminum cylinder with a radius of 50 nm, whereas in the case of infinite cladding the limit consists of a homogeneous aluminum space. While for $R\to 0$ the curves of the TE and HE modes of the infinitely cladded waveguide tend to $\mathrm{Im}\{\kappa_{alu}\}=0$, those of a finitely cladded waveguide are attracted by

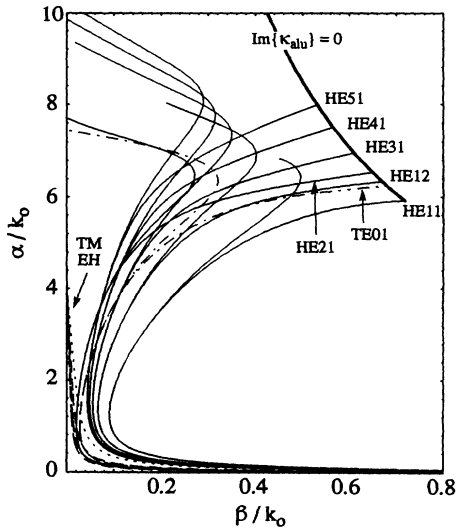

FIG. 14. Comparison between a finite cladding $D=50$ nm and an infinite cladding for the aluminum cladded dielectric waveguide. The figure shows parametric plots of the propagation constants (the core radius is the parameter). The HE and TE modes of the finitely cladded waveguide are attracted by the line $\beta=0$. The EH and TM modes are almost insensitive to the cladding thickness. Wavelength $\lambda=488$ nm; aluminum cladding $\varepsilon=-34+i8.5$; dielectric core $\varepsilon=2.16$; surrounded by vacuum.

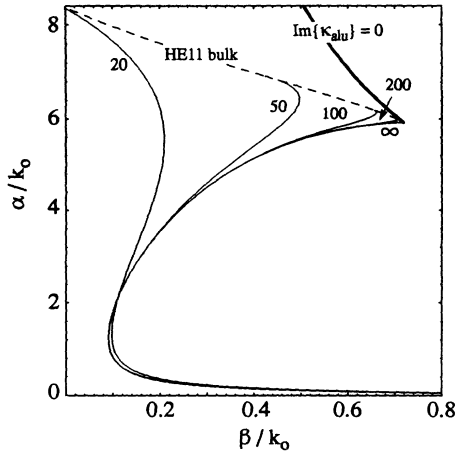

FIG. 15. Influence of cladding thickness on the HE11 mode. The figure shows parametric plots of the propagation constants of the HE11 mode (the core radius is the parameter). The numbers indicate the cladding thickness in nm. Wavelength $\lambda=488$ nm; aluminum cladding $\varepsilon=-34+i8.5$; dielectric core $\varepsilon=2.16$; surrounded by vacuum.

$$\mathrm{Im}\{\kappa_{vac}\}=0\ . \tag{17}$$

HE and TE modes with finite cladding therefore have cutoffs if the condition (17) can be fulfilled. Modes for which (17) cannot be fulfilled converge into the corresponding bulk modes of the aluminum cylinder. In Fig. 14 HE41 and higher modes have a cutoff, whereas HE11, HE21, and HE31 become bulk modes for $R\to 0$. Figure 15 shows a parametric plot of HE11 modes for different cladding thicknesses. For $R\to 0$ the propagation constants converge toward the corresponding bulk mode value, which is visualized by the dashed line taken from Fig. 10. If the cladding is too thin, the HE11 mode runs into cutoff at $\beta=0$ since the bulk mode has a low cutoff. In Fig. 16 the influence of finite cladding on the field distribution is shown for $R=8$ nm and $D=50$ nm.

EH and TM modes remain almost unaffected by the finite cladding, as seen in Fig. 14. Their propagation constants again cross the imaginary axis at $k_z\approx i4k_0$ which determines their cutoff for small R.

Surface modes of the finite cladding waveguide have in principle the same behavior as discussed for the metal wire. For certain values of R, however, the phase constants of a surface mode and a guided mode can come close to each other. If in addition both of them have the same symmetry, i.e., the same order n, coupling between these modes can be observed in an analog way to the coupling between dielectric waveguides [15]. For the slab waveguide the coupling between guided modes and lossy surface plasma waves is reported in Ref. [25]. It was shown that this coupling sensitively depends on layer thickness and that it is accompanied by a resonant absorption peak. Since there are two independent geometrical parameters for the present cylindrical structure, core radius R and cladding thickness D, we consider in the following a constant value for D. In Fig. 17 the coupling between surface and guided modes is shown for $n=1$ as a

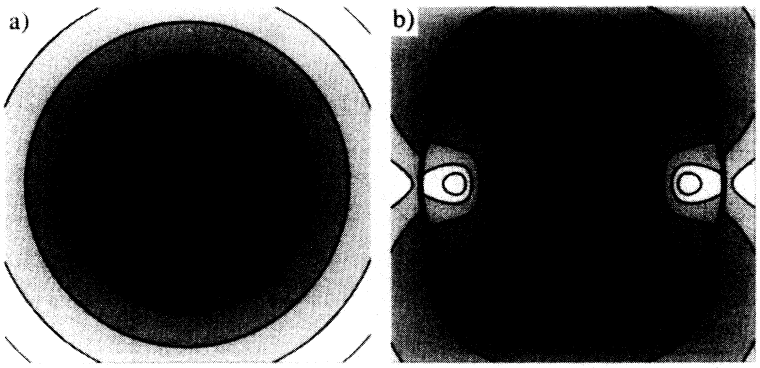

FIG. 16. Influence of finite cladding on the power distribution of the HE11 mode. Constant factor between successive contour lines. Core radius $R=8$ nm; wavelength $\lambda=488$ nm; aluminum cladding $\varepsilon=-34+i8.5$; dielectric core $\varepsilon=2.16$. (a) Infinite cladding; (b) cladding thickness $D=50$ nm; surrounded by vacuum.

function of R at a fixed cladding thickness $D=50$ nm. Near $R=109$ nm the β curve of the HE1 surface mode crosses the β curve of the HE11 guided mode. For this value of R the attenuation of each mode is far from each other. Nevertheless, a slight response due to coupling with the HE11 guided mode can be observed on the attenuation curve for the HE1 surface mode. Mode coupling becomes more pronounced for $R=255$ nm, where the phase constants of the HE1 surface and the EH11 guided modes intersect. In this case the attenuation constants are closer to each other than before and a much higher response can be observed. Finally at $R=376$ nm, a new, rather surprising coupling mechanism can be observed: the HE1 surface mode transforms into the HE12 guided mode and vice versa. This mode conversion is shown in more detail in the closeups of Fig. 17. For a radius $R=490$ nm, the HE12 guided mode which has now the characteristics of the HE1 surface mode transforms into the EH12 guided mode. This procedure continues for all higher guided modes of order $n=1$. A guided mode therefore transforms into the surface mode and finally transforms back into the next higher guided mode of the same order.

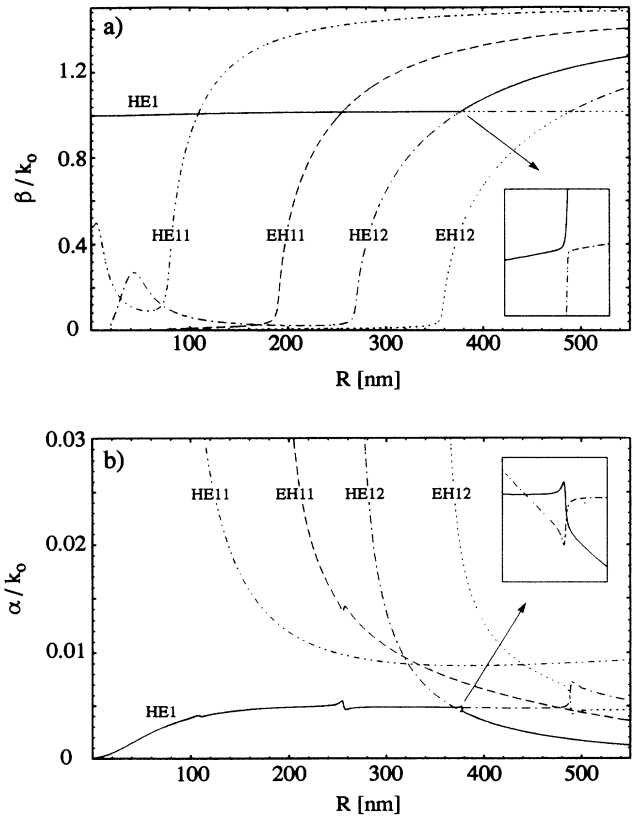

FIG. 17. Propagation constant as a function of core radius R for the modes of order $n=1$. The HE1 surface mode couples with the HE11 and EH11 guided modes and transforms into the HE12 guided mode (insets). Cladding thickness $D=50$ nm, wavelength $\lambda=488$ nm; aluminum cladding $\varepsilon=-34+i8.5$; dielectric core $\varepsilon=2.16$; surrounded by vacuum.

For orders $n>1$ similar behavior is observed. For $n=2$, for example, the HE2 surface mode cannot couple with the HE21 and EH21 guided modes because of its cutoff for $R\to 0$. Instead, it couples with the HE22 and then transforms into the EH22 guided mode. TE and TM modes for $n=0$ cannot couple since they are orthogonal to each other. The TM surface mode couples with the TM01 guided mode and then transforms into TM02 guided mode. For all mode conversions it is observed that the phase constants do not intersect whereas the α curves intersect twice (see inset in Fig. 17).

For large R, three different asymptotic limits are found, which are the same as those previously obtained in Secs. III and IV [cf. Eqs. (9), (10), and (15)]. These limits correspond, respectively, to guided, interface, and surface modes.

B. Frequency dispersion

So far, coupling between modes was limited to a fixed frequency. Of course, the same analysis can be done by varying the frequency and keeping R and D fixed. The frequency dispersion for $n=1$, $R=100$ nm, and $D=50$ nm is shown in Fig. 18. Although a large number of guided modes exists, only one is shown in the figure. This guided mode transforms at $\omega\approx 0.4\omega_p$ into the HE1 surface mode and vice versa. The HE1 interface mode, localized between core and cladding, remains unaffected. The mode conversion is shown in more detail in the inset of Fig. 18. In the nonradiative region, the behavior is very similar to frequency dispersion of a double-interface system. Interface modes could therefore be excited by

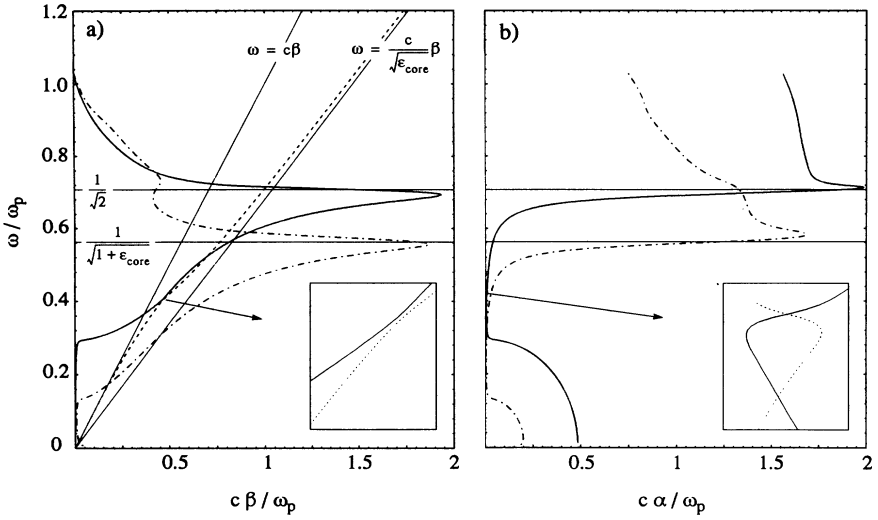

FIG. 18. Frequency dispersion of the HE1 surface mode, the HE1 interface mode, and a guided mode of order $n=1$. The HE1 surface mode and the guided mode (solid and dashed lines) transform into each other (insets). Core radius $R=100$ nm, cladding thickness $D=50$ nm, aluminum cladding $\hbar\omega_p=15.565$ eV, $\hbar\gamma=0.608$ eV; dielectric core $\varepsilon=2.16$; surrounded by vacuum.

the ATR method, in a way similar to that in experiments on metal layers of finite thicknesses [26].

Strong coupling between the two surface waves may be expected when the layer thickness becomes comparable to the radial decay lengths of the surface mode fields in the aluminum cladding. However, to keep the discussion in bounds, the influence of R and D on frequency dispersion is not further investigated. Note that mode conversion as a function of frequency behaves on principle similarly to mode conversion as a function of R: the phase constants repel while the α curves intersect twice.

VI. CONCLUSION

To understand light propagation in circular dielectric waveguides with finite metal cladding, three different waveguide structures have been discussed. The consideration of the finite damping of the metal leads to a continuous transition from propagating to evanescent guided modes. For large core radius or high frequencies, some guided modes become surface modes localized between dielectric core and metal cladding. Other surface modes are localized on the boundary between metal cladding and surrounding vacuum. For every order n, both types of surface modes are found to be single valued. Below the plasmon frequency they behave similarly to the Fano modes of a planar interface. Above the plasmon frequency, they convert into evanescent modes with very short propagation lengths. Surface and guided modes can either couple between each other or transform into each other. The latter occurs when in addition to the phase constants, the attenuations of both modes also come close.

With the exception of the HE11 guided mode and the HE1 surface mode, all the modes exist only above a critical frequency or a critical core radius. This cutoff behavior is on principle different from cutoff in dielectric waveguide theory, where it is associated with the abrupt transition from propagating to evanescent modes. In waveguides with lossy media no other modes are generated when cutoff is reached. When the core radius decreases, one solution after the other vanishes, until only the HE11 guided mode and the HE1 surface mode remain as solutions. At cutoff the argument of the Hankel function becomes real, indicating that the modes become purely radiative. The finite cladding mainly influences HE and TE modes; EH and TM modes remain almost unaffected.

Surface plasmon modes may be of importance for SNOM improvements. Near the plasmon frequency the HE1 surface mode is strongly localized at the surface of the metal coating. In addition, it has no cutoff, is only slightly sensitive to geometrical alterations, and has low attenuation. Instead of a tapered metal coated dielectric waveguide a simple metal tip with suitable material properties could be used as SNOM probe. How to excite such a mode near the plasmon frequency remains an open question. On the other hand, the HE1 surface mode at the interface core/cladding could be excited by ATR techniques. This mode, however, is rather sensitive to the core radius and is transformed into the HE11 guided mode below a certain radius or frequency.

Future work will concern the investigation of additional waveguide structures such as waveguides with two metallic domains. Transmission line theory predicts no cutoff for such a configuration. In addition, an arrangement operating with the plasmon mode localized between the metallic domains would be able to strongly focus light and would therefore represent a powerful SNOM probe.

ACKNOWLEDGMENTS

The authors wish to thank D. W. Pohl and O. J. F. Martin for instructive cooperation and for many useful and illuminating discussions.

[1] *Near Field Optics,* Vol. 242 of *NATO Advanced Study Institute, Series E,* edited by D. W. Pohl and D. Courjon (Kluwer, Dordrecht, 1993).
[2] L. Novotny, D. W. Pohl, and P. Regli, J. Opt. Soc. Am. A **11**, 1768 (1994).
[3] See, for instance, E. N. Economou and K. L. Ngai, in *Aspects of the Study of Surfaces,* Advances in Chemical Physics Vol. 27, edited by I. Prigogine and S. A. Rice (Wiley, New York, 1974), pp. 265–354.
[4] *Electromagnetic Surface Modes,* edited by A. D. Boardman (Wiley, Chichester, 1982).
[5] J. R. Sambles and R. A. Innes, in *Surface Plasmon-Polaritons,* IOP Short Meetings Series Vol. 9 (Institute of Physics and Physical Society, Bristol, 1987), pp. 121–138.
[6] H. Khosravi, D. R. Tilley, and R. Loudon, J. Opt. Soc. Am. A **8**, 112 (1991).
[7] G. C. Aers, A. D. Boardman, and B. V. Paranjape, J. Phys. F **10**, 53 (1980).
[8] C. A. Pfeiffer, E. N. Economou, and K. L. Ngai, Phys. Rev. B **10**, 3038 (1974).
[9] J. C. Ashley and L. C. Emerson, Surf. Science **41**, 615 (1974).
[10] R. Ruppin, in *Electromagnetic Surface Modes,* edited by A. D. Boardman (Wiley, Chichester, 1982), pp. 345–398.
[11] C. Miziumski, Phys. Lett. **40A**, 187 (1972).
[12] S. S. Martinos and E. N. Economou, Phys. Rev. B **28**, 3173 (1983).
[13] B. Prade and J. Y. Vinet, J. Lightwave Technol. **12**, 6 (1994).
[14] R. E. Collin, *Field Theory of Guided Waves* (IEEE, New York, 1991).
[15] D. Marcuse, *Light Transmission Optics* (Krieger, Malabar, 1989).
[16] NAG Fortran Library, Numerical Algorithms Group Ltd., Oxford (UK), 1990.
[17] Ch. Hafner, *2-D MMP: Two Dimensional Multiple Multipole Analysis Software and User's Manual* (Artech, Boston, 1990).
[18] C. F. Bohren and D. R. Huffmann, *Absorption and Scattering of Light by Small Particles* (Wiley, New York, 1983), Chap. 9.4.
[19] *Handbook of Mathematical Functions,* 9th ed., edited by M. Abramowitz and I. A. Stegun (Dover, New York, 1972).
[20] E. T. Arakawa, M. W. Williams, R. N. Hamm, and R. H. Ritchie, Phys. Rev. Lett. **31**, 1127 (1973).
[21] P. Halevi, (Ref. [10]), pp. 249–304.
[22] S. A. Rice, D. Guidotti, and H. L. Lemberg, in *Aspects of the Study of Surfaces,* Advances in Chemical Physics Vol. 27, edited by I. Prigogine and S. A. Rice (Wiley, New York, 1974), pp. 543–633.
[23] D. Hondros, Ann. Phys. (Leipzig) **30**, 905 (1909).
[24] K. L. Kliewer and R. Fuchs, in *Aspects of the Study of Surfaces,* Advances in Chemical Physics Vol. 27, edited by I. Prigogine and S. A. Rice (Wiley, New York, 1974), pp. 355–541.
[25] J. N. Polky and G. L. Mitchell, J. Opt. Soc. Am. **64**, 274 (1974).
[26] K. Welford, in *Surface Plasmon-Polaritons,* IOP Short Meetings Series Vol. 9 (Institute of Physics and Physical Society, Bristol, 1987), pp. 25–99.

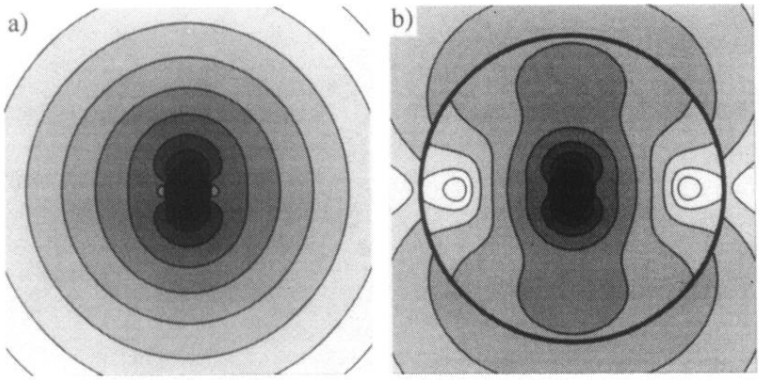

FIG. 16. Influence of finite cladding on the power distribution of the HE11 mode. Constant factor between successive contour lines. Core radius $R = 8$ nm; wavelength $\lambda = 488$ nm; aluminum cladding $\varepsilon = -34 + i8.5$; dielectric core $\varepsilon = 2.16$. (a) Infinite cladding; (b) cladding thickness $D = 50$ nm; surrounded by vacuum.

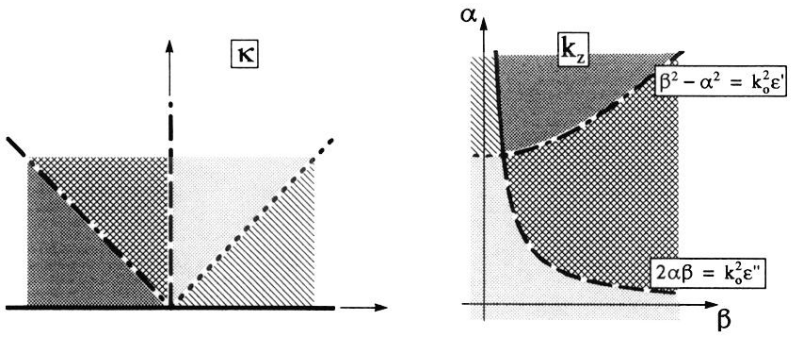

FIG. 3. Transformation from transverse wave number κ to propagation constant $k_z = \alpha + i\beta$.

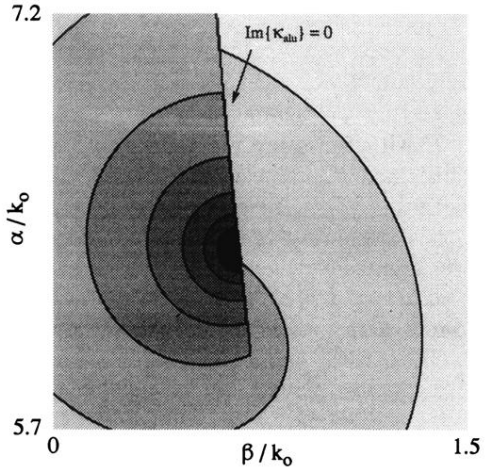

FIG. 4. Lines of constant $|\det[M(k_z)]|$. Core radius $R=20.5$ nm; wavelength $\lambda=488$ nm; infinite aluminum cladding $\varepsilon=-34+i8.5$; dielectric core $\varepsilon=2.16$. The minimum corresponds to the HE21 mode when reaching cutoff. The discontinuity indicates $\mathrm{Im}\{\kappa_{\mathrm{alu}}\}=0$.